Indian Geotech J
https://doi.org/10.1007/s40098-023-00777-6

ORIGINAL PAPER

Science and Technology of Additive Manufacturing Applied to Geotechnical Engineering

Gali Madhavi Latha[1] · Hasthi Venkateswarlu[1] · Prerana Krishnaraj[1] · Sai Kumar Allam[1] · K. V. Anusree[1] · Aarya Krishna[1]

Received: 26 December 2022 / Accepted: 6 September 2023

Abstract The ability and freedom to translate complex conceptual creations into designs and prototypes using simple digital and mechanical tools make additive manufacturing (3D printing) attractive and rewarding to all fields that involve manufacturing. Though 3D printing is rapidly spreading into all fields of engineering and science, its scope in geotechnical engineering is so far confined to limited materials, which are primarily manufactured to aid small-scale modelling and research. While serious prototyping is still far, optimization of 3D printing parameters for different applications, which is a niche requirement for the spread of this technology, is not given serious consideration so far. As a first step in this direction, this study explores the methods and applications of 3D printing for geotechnical manufacturing processes and focuses on the importance of optimization of 3D printing parameters. Two vibrant manufacturing processes of geotechnical engineering, namely production of geosynthetics and manufacturing of sand, were selected for this study. Polymeric sheets of different surface texture and geogrids of different aperture sizes and shapes were printed using fused deposition modelling (FDM) printing technique. Two different raw materials, polypropylene for polymeric sheets and polylactic acid for geogrids, were used. The surface texture of the polymeric sheets was altered by choosing horizontal, diagonal, and vertical orientations of printing layers. Geogrids of square, circular, and triangular apertures were printed. The study demonstrated the clear effects of printing direction and printing material on the mechanical response of the products, which were understood through tension tests and interface shear tests. Further, granular particles of different sizes and same shape were 3D printed using two different printing techniques, namely FDM and stereolithography. Effectiveness of both these techniques in closely replicating the morphology of the natural sand particles used to create their polymeric twins using 3D printing was compared. The study provides fundamental understanding of 3D printing techniques related to geotechnical engineering along with their parametric dependency and lays out the futuristic applications and limitations of this field.

Keywords 3D printing · Additive manufacturing · Geosynthetics · Geogrid · Sand · Mechanical response

Background

Additive manufacturing, which is also known as 3D printing, provides exciting opportunities to all domains of scientific investigations and applications. 3D printing has emerged as a revolutionary technique in many industries due to its numerous capabilities, including mass customization, quick prototyping, waste minimization, flexibility, and diversity in design. This method involves printing consecutive layers of material on top of each other. Charles Hull created this technology in 1986 using a procedure called stereolithography (SLA), which inspired the creation of all other 3D printing techniques [1]. The advancement in 3D printing technology resulted in the development of different processes and materials to suit different applications. Prior to the adoption of 3D printing for a certain application, background knowledge of various 3D printing processes and materials is essential. The currently available 3D printing processes

✉ Gali Madhavi Latha
madhavi@iisc.ac.in

Hasthi Venkateswarlu
hvenkateswar@iisc.ac.in

[1] Department of Civil Engineering, Indian Institute of Science Bangalore, Bangalore, India

Published online: 25 September 2023

are categorized into seven types. They are material extrusion, direct energy deposition, material jetting, powder bed fusion, vat photopolymerization, binder jetting, and sheet lamination. The schematic representation of all these processes is shown in Fig. 1.

The material extrusion process follows the extrusion of filament material using nozzle for printing the object. Fused deposition modelling (FDM) and direct ink writing (DIW) methods follow this principle. All types of plastics can be used as raw materials for FDM printing, whereas only hydrogels are used in DIW printing. In the process of direct energy deposition, numerous high energy sources like lasers and electron beams are used to melt the metals to print the objects. Laser Engineered Net Shaping (LENS) and Electron Beam Welding (EBW) methods come under this process. Multi-Jet Modelling (MJM) consists of deposition and solidification stages. Initially, liquid droplets of wax or photopolymer resin are jetted onto the building platform and subsequently these droplets are cured into solids using ultraviolet (UV) light. Polyjet or inkjet printing methods are examples of this process. Powder bed fusion process involves melting or sintering of the powdered materials using energy sources like laser and electron beam. 3D printing techniques like selective laser sintering (SLS), selective laser melting (SLM), and electron beam melting (EBM) follow powder bed fusion process. In the vat photopolymerization process, raw materials in liquid form are solidified by the polymerization of a resin or plastic with the help of a light source. This process is followed in SLA printing. In binder jetting process, models are created by depositing the liquid binding agent onto a thin layer of numerous powder particles like ceramics, foundry sand, and composites. Indirect inkjet printing (IIP) method uses this principle. Sheet lamination process consists of cutting and assembling of solid materials using ultrasonic welding or compaction for building the model. Ultrasonic additive manufacturing (UAM) and laminated object manufacturing (LOM) methods are the examples of this process. The literature suggests that majority of the studies in the field of geotechnical engineering employed FDM printing. Thompson et al. [2] compared the usage of different 3D printing techniques for soil science applications. As per their study, 36% of the total number of studies reported on soil science applications till 2016 have used FDM printing technique, as shown in Fig. 2a. Application of 3D printing techniques were found in protecting cultural and natural heritage, providing sources for raw materials made of minerals like clay, sand, and gravel, preserving soil biodiversity, storage and circulation of water, and infrastructure development. In total, FDM and material jetting methods (MJM) cover 66% of overall utilization of different 3D printing methods.

Apart from identifying the 3D printing process, selection of suitable printing material is important for creating parts with desired physical, mechanical, and functional

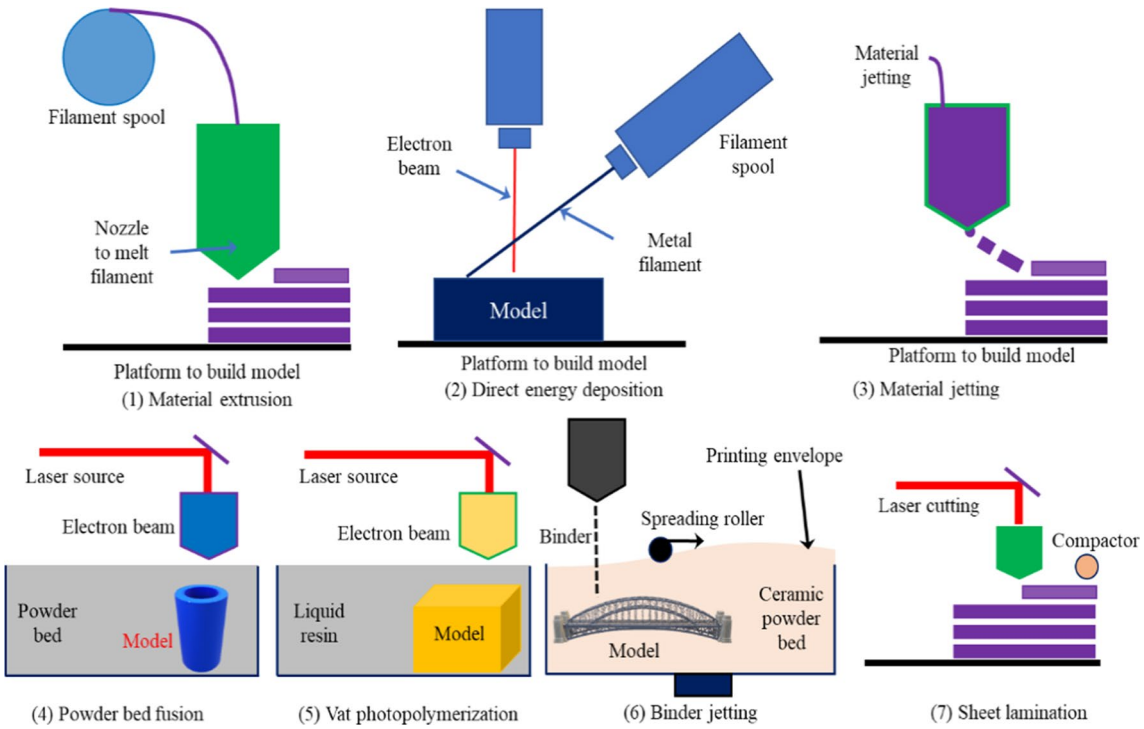

Fig. 1 Schematic representation of currently available 3D printing processes

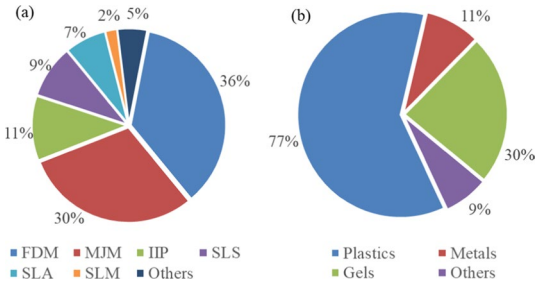

Fig. 2 The presence of different 3D printing applications in soil science **a** usage of 3D printing methods; **b** usage of 3D printing materials (data source: Thompson et al. [2])

characteristics. The selection of raw material mainly depends on the printing method. At present, limited freedom can be exercised on the raw material selection based on the intended use of the printed product. Popularly used printing materials are plastics, which can be further divided into thermosetting (e.g. polyesters, silicone-based, and epoxy materials) and thermoplastic (i.e. polylactic acid, polyamide, polypropylene, and polyethylene), metals (titanium, stainless steel, aluminium, and nickel alloys), resins (rigid and elastomeric polyurethane) and other materials like graphene-based materials, biomaterials, silicon-based materials including ceramics, and glass [2]. Plastics are the most used raw materials for 3D printing, as shown in Fig. 2b. The reason for their domination is their suitability for commonly used 3D printing processes like FDM, MJM, and SLA. The advantages and limitations of three most used raw materials of 3D printing are given in Table 1. Interestingly, there is a lack of studies demonstrating the application of biobased materials.

Application of 3D Printing in Geotechnical Engineering

Substantial portion of 3D printing-related research in geotechnical engineering is related to the understanding of mechanical and hydraulic behaviour of geomaterials. Many available studies are focused on examining the behaviour of 3D-printed soil analogues and reinforcing materials from the perspective of geotechnical engineering. The rapid evolution of 3D printing technology and its ability to have total control on design features allowed the researchers to easily print materials with desirable geometrical features for testing.

One of the primary uses of 3D printing technology in geotechnical engineering is to print particles mimicking the size and shape of the granular particles. Since 3D printing gives the power to individually adjust the morphological features of grains including gradation, size, and shape, considerable number of studies were carried out on 3D printed granular soils [3]. Miskin and Jaeger [4] demonstrated that 3D-printed analogue particles accurately mimic the morphology of natural sand particles. Triaxial tests on 3D-printed sand particles revealed that they exhibit stress-dilatancy behaviour, closely resembling that of the natural soils [5]. Further, compression tests on natural and 3D-printed particles revealed that 3D-printed particles qualitatively resemble essential components of compression behaviour of natural soils, such as compression and recompression indices [6]. Based on the findings from bender element tests, shear wave velocity and shear modulus of 3D-printed particles were found to be very close to those of the natural sands [5].

Other potential applications of 3D-printed analogues include studying the frictional behaviour of faults, simulating the crack pattern of different rock materials, calibrating DEM simulations, and understanding the gradation effects on the hydraulic conductivity of granular soils [7]. While the findings from several laboratory-scale studies demonstrated the usefulness of 3D-printed synthetic soils as soil substitutes that offer a great degree of control over their characteristics to assist in advanced research, low stiffness of the printed particles poses a great challenge for the use of these particles to load-bearing applications. Ahmed and Martinez [5] reported that despite the lower stiffness of 3D-printed particles, they imitate many of the functional trends and behavioural patterns of natural soils. Going forward, the 3D printing technology will hopefully advance to print stiffer and stronger soil particles to exactly replicate the natural soils.

Table 1 Comparison of different raw materials of 3D printing

Material type	Advantages	Limitations	Primary application
Plastics	Rapid prototyping, mass customization, economic efficiency, and ability to create complex forms	Anisotropic mechanical properties, limited variety	Construction and infrastructure
Metals	Scope for functional optimization, improved material utilization and easy assembling and repair	Limited alloys, dimensional inaccuracy, poor surface finish, tedious post-processing	Medium-scale components for a variety of applications
Resins	Mass production, fine surface finish and ability to create complex geometries	Limitations on product size, accuracy constraints	Jewellery, engineering, and medical applications

A few researchers have used 3D printing technology to print soil reinforcing elements for laboratory studies. Arab et al. [8] used 3D-printed geogrids of honeycomb-shaped cellular apertures for improving the load bearing capacity of sand. Geometric features of cells and stiffness of the geogrids were varied in plate load tests on sand reinforced with geogrids to suggest that a maximum bearing capacity ratio of 1.59 can be achieved through optimized cell dimensions. Chalmovsky et al. [9] used 3D-printed synthetic fibres to reinforce clays. Drained triaxial tests on reinforced clays reinforced with 3D-printed fibres of varying shape showed that profiled fibres provide superior reinforcement than the straight fibres.

The field of 3D printing is expanding quickly, and the technology is evolving into futuristic manufacturing technology, encompassing many materials and methods to closely resemble the materials of interest. It is not very far that many manufacturing processes of geotechnical engineering will be replaced by this additive manufacturing, providing plenty of opportunities to researchers and engineers of this stream. With such advancement, most elusive geotechnical processes like pore connectivity, tortuosity, inter-grain and interface contact mechanics, contaminant migration and fracturing can be investigated and explained with a better prognosis.

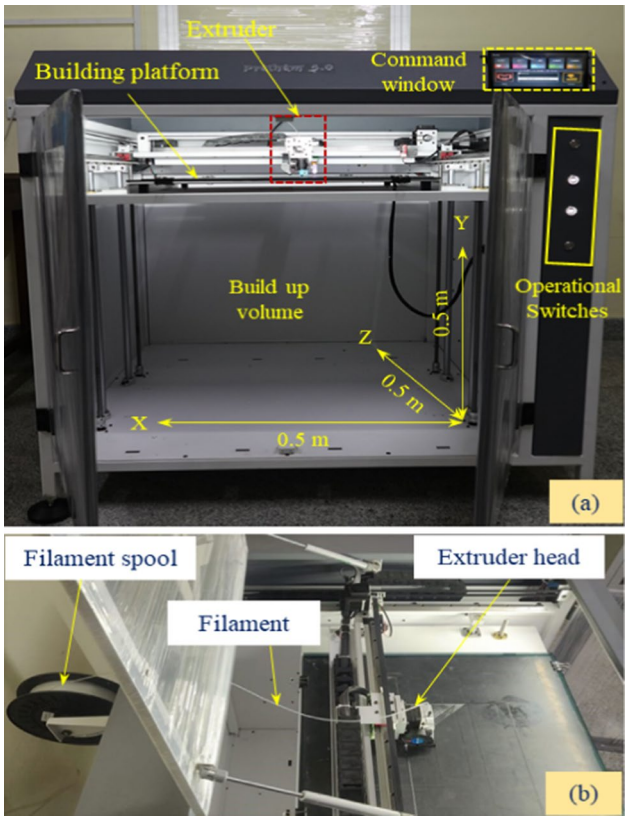

Fig. 3 FDM printer **a** major components; **b** printing mechanism

Objectives of the Study

The current study is focused on understanding the level to which 3D-printed geomaterials can mimic the natural materials and to demonstrate their usage in applications related to soil reinforcement and granular mechanics. The study is mainly focused on 3D printing of geosynthetics and understanding their mechanical response. Two different geosynthetics, namely planar sheets and geogrid, were manufactured using 3D printing. Surface texture of planar geosynthetic sheets was varied by tweaking the printing parameters. In case of geogrids, aperture shape was varied. A series of tensile tests and interface direct shear tests were carried out to demonstrate the mechanical response and interface behaviour of 3D-printed geosynthetics. Further, a small part of the study is focused on understanding the effectiveness of different printing methods in reproducing the morphology of natural sand particles.

3D Printing of Geosynthetics

Two different geosynthetics, namely planar sheets and geogrid, were manufactured using fused deposition modelling (FDM)-based printer shown in Fig. 3a. Melting and bonding of a continuous thermoplastic filament are the basis of the FDM fabrication process. The major components of the printer are operational switches, command window, extruder, building platform, and filament spool holder.

Operational keys are used to turn on, off, and reset the printer. Command window provides control to printing parameters, namely heating temperature of filament, position and movement of the building platform. Design of the printing object prepared through computer-aided design (CAD) can be supplied to the printer through a flash drive or directly from a computer. Raw printing material in the form of wire-shaped filament from the spool is fed to the extruder. The filament spool of required raw material is setup prior to printing. According to the supplied design, the extruder moves for printing the model. The filament melts inside the extruder and with the movement of the extruder, the melted filament gets deposited over the building platform. The melted filament cools down to room temperature, and the product with required design gets ready on the building platform.

In this study, polypropylene (PP) and polylatic acid (PLA) filaments were used to print the planar sheets and geogrids, respectively. Heating temperatures of PP and PLA filaments are 240 °C and 220 °C, respectively. Planar sheets were printed with three different printing orientations, namely horizontal, diagonal, and vertical to obtain three different surface textures. Printing speed was selected as 30 mm/s,

based on trials. The sheets were printed to a thickness of 0.2 mm in two layers, each layer of thickness 0.1 mm. Figure 4a shows the 3D-printed geosynthetic sheet on the building platform, and Fig. 4b shows the microscopic images of printed sheets at different printing orientations, taken at 16× magnification.

Figure 5a shows the 3D printing of geogrids. In case of geogrids, the thickness was kept as 1.2 mm and the aperture shape was varied as circular, square, and triangular, as shown in Fig. 5b. Aperture size of the square geogrid was kept as 4.8 mm × 4.8 mm. Keeping this as the basis for the aperture area of the geogrids being printed, the aperture sizes of circular and triangular geogrids were determined. Thus, the equivalent aperture area of each geogrid is identical.

Mechanical Response of 3D-Printed Geogrids

The tensile behaviour of 3D-printed planar sheets and geogrids and their interface behaviour with sand were studied through tensile tests and interface direct shear tests, respectively.

Tensile Response

Strip tensile test was performed on planar geosynthetic sheets printed in different orientations. Tests on sheets were carried out as per the guidelines of ASTM D-882 [10], and tests on grids were carried out as per ASTM D-6637 [11]. All tests were conducted at a strain rate of 10 mm/min using a universal testing machine, as shown in Fig. 6.

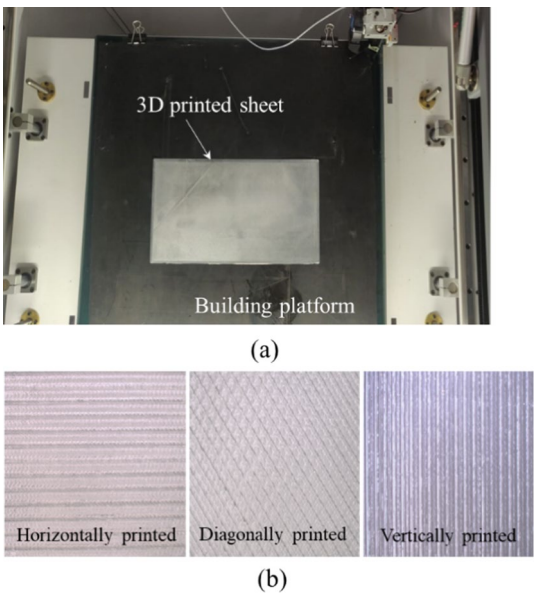

Fig. 4 3D printing of planar sheets **a** printed sheet, and **b** variation in surface texture

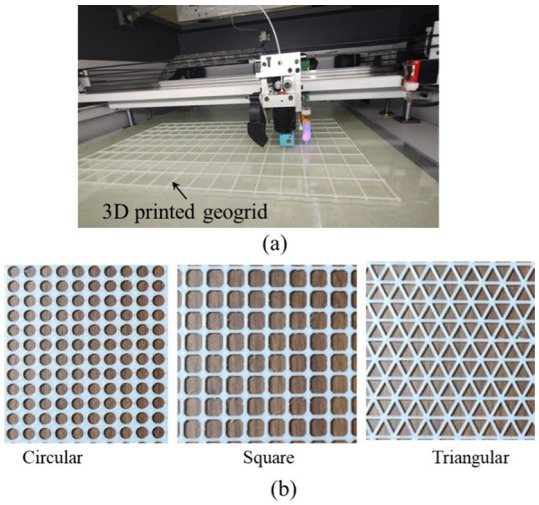

Fig. 5 3D printing of geogrids **a** printed geogrid, and **b** different aperture shapes

Figure 7 shows the results of tension tests on planar sheets and geogrids. The direction of tension is orthogonal to the direction of fused planar layers in case of horizontally printed sheets, parallel to the direction of layers in case of vertically printed sheets and inclined at 45° in case of diagonally printed sheets.

As shown from Fig. 7a, diagonally printed planar sheets showed highest tensile strength, followed by vertical and horizontal sheets. The initial tangent modulus was determined as 180.5 MPa, 431.8 MPa, and 413.6 MPa, respectively, for horizontal, diagonal, and vertical sheets. The difference in the tensile strength and stiffness is mainly due to the process of printing. In case of diagonal sheets, the second layer is fused in orthogonal direction to the first fused layer, as shown in Fig. 4b. In other two cases, both the layers are fused in the same direction and get overlapped, creating clear planes of weakness between the successively fused

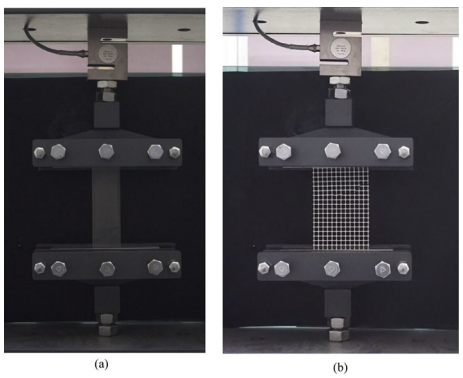

Fig. 6 Tensile testing of 3D-printed geosynthetics **a** planar sheet, and **b** geogrid

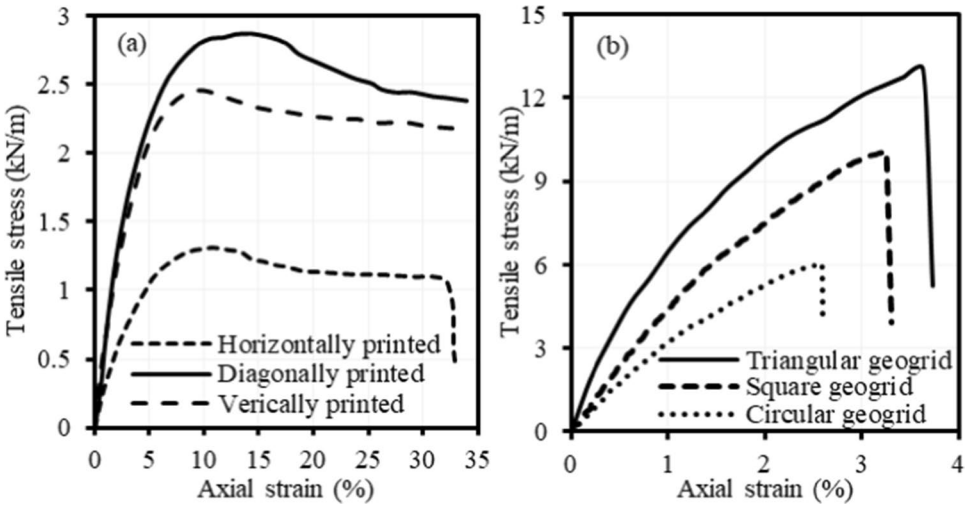

Fig. 7 Tensile response of 3D-printed geosynthetics **a** planar sheet, and **b** geogrid

layers. Since these planes of weakness are orthogonal to the pulling direction in case of horizontally fused sheets, these sheets give away easily in tension due to the separation of fused layers. In case of vertically fused sheets, the planes of weakness and the fused layers are aligned with the direction of pull and hence the tensile strength is mainly derived from the fused filament, the planes of weakness not getting stretched in the weaker direction to get separated. Since the strength of the filament is higher than the bonding between the fused layers, vertically printed sheets exhibited higher tensile strength than the horizontally printed sheets.

Response of geogrids in tension tests is shown in Fig. 7b. Peak tensile strength was found to be maximum for geogrids with triangular aperture compared to grids with square and circular apertures. By virtue of its shape, triangular grid offers isotropic resistance against the tensile load in all three directions. Tensile resistance is limited to two directions in case of square geogrids, and hence, their tensile strength is lower than that of the triangular grids. In case of geogrids with circular apertures, it was easy to expand the circular aperture through tensile pull because the expansion of the aperture happens in the direction of tensile pull, leading to quick weakening of the grid. Hence, the tensile strength of the circular grid was less than 50% of that of the triangular grid.

Interface Shear Response

The shear response of sand–planar sheet and sand–geogrid interfaces was studied through a series of displacement-controlled interface direct shear tests. The setup used for the interface direct shear tests is shown in Fig. 8. A shear box of 80 mm × 80 mm × 50 mm size was used for these tests (Fig. 8a), and the rate of horizontal displacement was maintained as 1.25 mm/min. In case of sand–planar sheet interfaces, shear box filled with sand was positioned over the

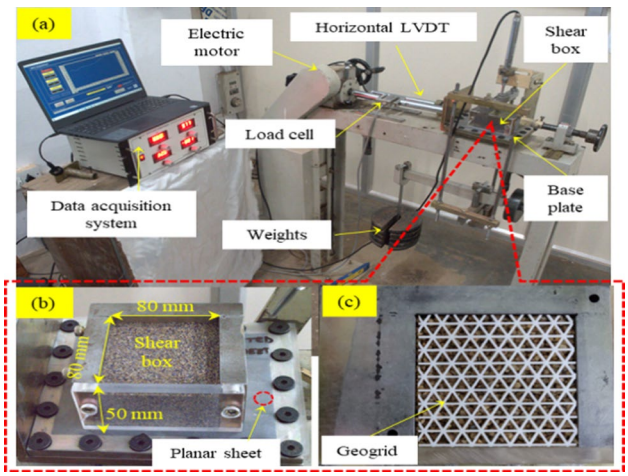

Fig. 8 Interface direct shear test setup: **a** major parts; **b** arrangement for sand–sheet interface tests **c** arrangement for sand–grid interface tests

planar sheet, which is fixed to a rigid steel base plate with bolting arrangement, as shown in Fig. 8b. No bottom shear box is used for these tests. This arrangement arrests sagging of geosynthetic sheets during testing and ensures that shearing takes place exactly along the sand-geosynthetic plane. In shear tests with grids, upper and lower boxes filled with sand were used with the geogrid placed at the interface, as shown in Fig. 8c. Since geogrids are stiffer, this arrangement works better for shearing the sand–geogrid interfaces. Tests were carried out at normal stresses of 40 kPa, 80 kPa, and 120 kPa for all interfaces. At each normal stress, load and displacement were recorded using the load cell and the LVDT, respectively.

Sand used in the interface direct shear tests was classified as uniformly graded sand with letter symbols SP, as per the Unified Soil Classification System. The minimum and

maximum dry unit weights of the sand were determined as 13.65 kN/m^3, and 15.75 kN/m^3, respectively. The relative density of the sand was maintained as 90% in all the tests to represent the densely compacted field condition. The cohesion and internal friction angle of the sand were determined as 0.6 kPa, and 37°, respectively, from the direct shear tests. The shear response of different sand–planar sheet interfaces is shown in Fig. 9. The horizontally printed PP sheets produced the lowest peak shear stress among the three different types of sheets.

To quantify the effect of orientation on shear strength, interface coefficient (τ), which is the ratio between the peak shear strength of sand–planar sheet interface to the peak shear strength of sand–sand interface was determined for all interfaces. The τ value of sand–planar sheet interfaces for horizontal, vertical, and diagonal orientation was found to vary from 0.55 to 0.57, 0.87 to 0.91, and 0.89 to 0.92, respectively, with the change in normal stress from 40 to 120 kPa. The value of τ is 1 for sand–sand interface. During interface shear test, fused layers of vertical, diagonal, and horizontally printed sheets are aligned in orthogonal, diagonal, and parallel to the shearing direction, respectively. In case of horizontally printed sheets, sand particles simply slide over the fused layers without any interlocking, which resulted in low interface shear strength. In case of vertical and diagonally printed sheets, fused layers are orthogonal and diagonal to the shearing direction, and hence, particles get interlocked within the fused later texture, resulting in higher interface shear strength. It is very important to note that diagonally printed sheets showed τ value close to that of sand–sand interface, highlighting the advantages of using such texture for geosynthetic-reinforced soil structures.

Figure 10 shows the influence of aperture shape of geogrid on the shear response of sand–geogrid interfaces. The τ value of sand–geogrid interfaces with triangular, square, and circular apertures of the grid was between 0.82–0.89, 0.73–0.77, and 0.53–0.6, respectively, in the normal stress range of 40–120 kPa.

The τ value depends on the passive resistance offered by the geogrid against the movement of soil particles during the test. Though the effective opening size of all grids is the same, the triangular shape offers highest passive resistance due to the orientation of the ribs around the aperture. Since the ribs are diagonally crossing each other, sand particles cannot easily shear past these ribs and the effective interlocking in triangular shape is much higher compared to square

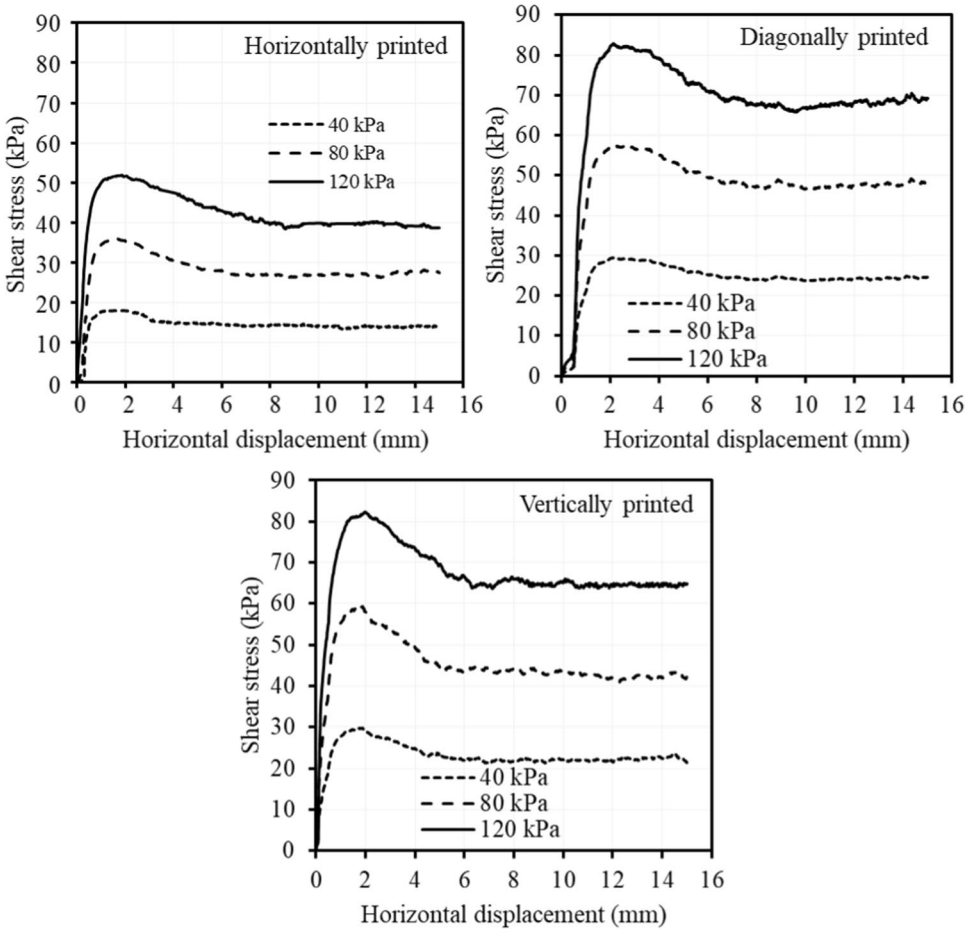

Fig. 9 Effect of printing orientation on the shear response of sand–planar sheet interfaces

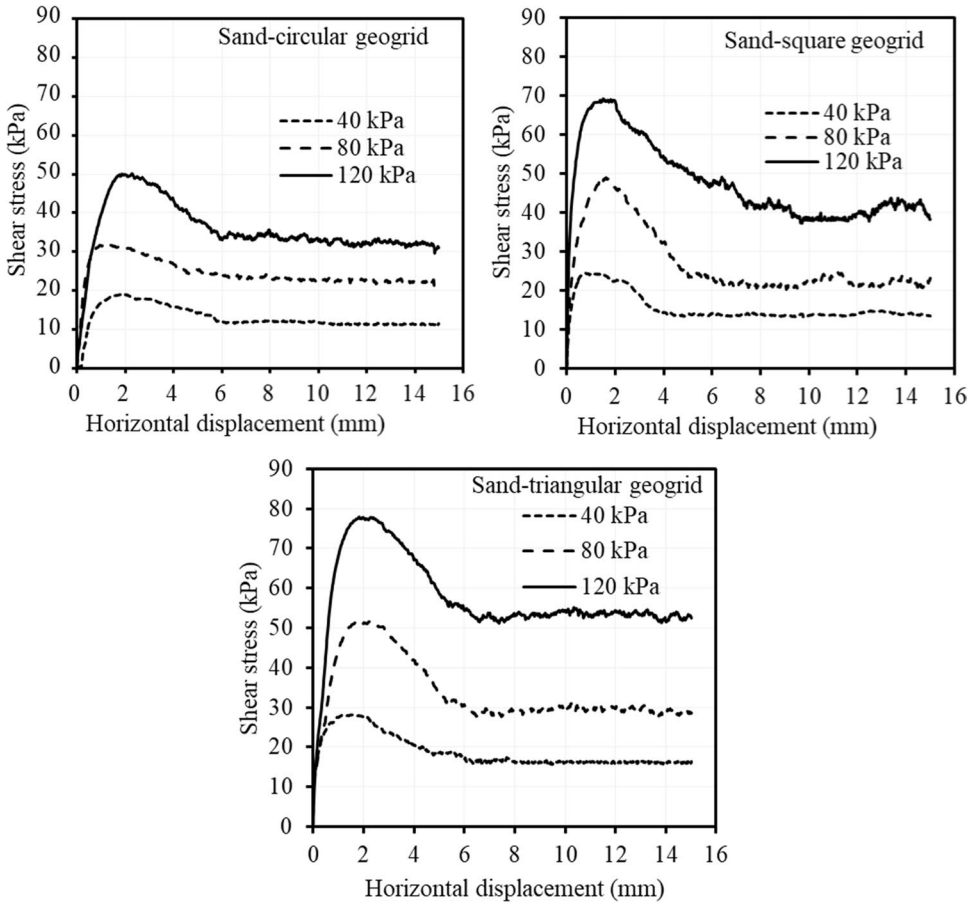

Fig. 10 Effect of aperture shape on the shear response of sand–geogrid interfaces

and circular grids. Hence, triangular grids offered comparatively greater passive resistance and resulted in higher τ values. Circular apertures are found to be least effective in interlocking the particles because of lack of sharp corners, thus resulting in least interface frictional strength.

Advantages and Limitations of 3D Printing of Geogrids

Since the manufacturing process and the raw materials differ in 3D printing and extrusion, the strength and stiffness properties of 3D-printed geogrids significantly differ from those of the extruded geogrids. After testing several commercial geogrids, Al-Omari and Fekheraldin [12] found that the stiffness of the extruded geogrids varies between 30 and 400 MPa. The stiffness of the geogrids printed in the current study is in the range of 176–334 MPa, which is comparable. Tensile properties of extruded biaxial geogrids tested by several researchers are summarized in Table 2. The literature suggests that the tensile strength of geogrids depends on several factors, including the properties of the base polymer, mass per unit area and thickness of the geogrid and the geometric features of the geogrid, including the aperture size. Though 3D printing offers multiple advantages over conventional extrusion process of geogrid manufacturing, the tensile strength of 3D-printed geogrids is limited by the raw materials that can be used with the current technologies. The use of high strength polymers for 3D printing is still in the research stage.

With the current state of 3D printing technology, printing geogrids are expensive and time consuming compared to the conventional extrusion process. However, the 3D printing process is less energy-intensive and uses simple machinery for production. Also, 3D printing can customize the geometric and structural features of geogrids easily for individual lots to revolutionize the geogrid manufacturing and produce millions of varieties of geogrids without creating any new machines. 3D printing process produces zero waste, unlike the extrusion process. The raw materials in 3D printing are plant-based polymers that can easily degrade. Hence, the objective of 3D printing in the current study is to produce customized geogrids in a sustainable way. Going forward, with the exponential growth of 3D printing industry, the processes will soon be cost and time effective.

3D Printing of Soil Particles

The physical, mechanical, and hydraulic behaviour of sands is greatly influenced by the morphological features

Table 2 Summary of tensile properties of extruded geogrids reported in the literature

Reference	Geogrid material	Aperture size of the geogrid	Ultimate tensile strength (kN/m)	Failure strain (%)
Guo et al. [13]	Polyamide	1.2 mm × 1.2 mm	14.00	16.6
Guo et al. [13]	Polyamide	1.5 mm × 1.5 mm	2.50	20.2
Phanikumar [14]	High-density polyethylene (HDPE)	6 mm × 6 mm	7.68	20.2
Latha et al. [15]	Non-oriented polymer	8 mm × 7 mm	7.50	55.0
Manohar and Anbazhagan [16]	Polyvinyl chloride (PVC)	9 mm × 9 mm	1.60	14.5
Naeini et al. [17]	HDPE	10 mm × 10 mm	7.60	50.0
Latha et al. [15]	HDPE	35 mm × 35 mm	20.00	25.0
Maghool et al. [18]	Polypropylene	39 mm × 39 mm	20.00	12.0

of the grains, such as size, shape, and surface roughness. Thus, the appropriate selection of printing mechanism is inevitable for reproducing the surface features of granular media. This section demonstrates the efficacy of two printing mechanism namely digital light processing (DLP) and stereolithography (SLA), in reproducing the desired shape of granular particles. A grain of size 7.07 mm × 5.802 mm × 3.602 mm in three orthogonal directions was considered as the model material for printing. The particle was printed using DLP and SLA at different scales. The particles were printed at scales of 0.6 and 4 using a DLP printer and at scales of 1.98, and 4 using an SLA printer. The dimensions of the sand grain corresponding the scales of 0.6, 1.98, and 4 are 4.243 mm × 3.481 mm × 2.161 mm, 14 mm × 11.49 mm × 7.13 mm, and 28.287 mm × 23.209 m m × 14.409 mm, respectively. Figure 11 shows the images of 3D-printed grains of different scales. It was not possible to print the particle scale less than 1.98 using SLA printer, whereas printing at a scale of 0.6 was possible using DLP. Particles printed using DLP needed post-printing UV curing process in a separate chamber to get the solidified shape. Hence, particles printed using DLP are much harder than particles printed using SLA, making them more suitable for applications that put certain amount of pressure on the particles.

To assess the effectiveness of printing mechanisms, 2D image analysis was carried out through developing an algorithm in MATLAB based on the method suggested by Vangla et al. [19]. Three alternative orientations referred to as Plane 1, Plane 2, and Plane 3 for each particle image were imaged to compute the shape parameters, as shown in Fig. 11e. Since taking the image at only one angle can lead to missing significant aspects of the particle morphology, three orientations were chosen to bring the study to as close to a 3D analysis. For the comparison of morphology, sphericity, and roundness [19] were calculated for both the natural and 3D printed particles and are listed in Table 3.

In each of the three planes, sphericity of all samples is comparable to that of the reference sand particle. It shows that distinct particles at the same scale may be precisely recreated without changing their form. SLA printer was not effective in recreating particles even at a scale of 1.98, whereas DLP was effective even for a smaller scale of 0.6, except for the discrepancy in roundness. However, when it comes to the particle proportions, both SLA and DLP printers produced satisfactory results. Particles printed at a scale of 4 using SLA and DLP printers precisely recreated the morphological features of the reference particle. These results reveal that SLA printing is not effective to print sand-sized particles. If scale effects are not important, for

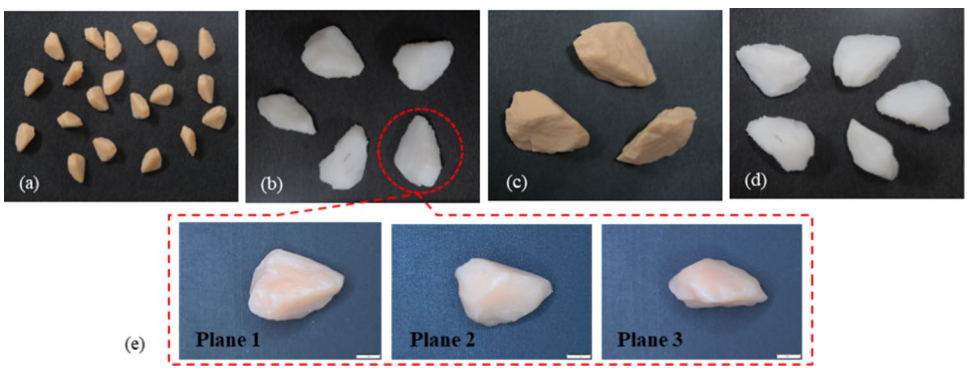

Fig. 11 3D-printed particles **a** at scale 0.6 using DLP, **b** at scale 1.98 using SLA, **c** at scale 4 using DLP **d** at scale 4 using SLA, and **e** different views of a typical 3D-printed particle

Table 3 Summary of the shape parameters of natural and 3D-printed particles

Particle type, scale	Printing technology	Sphericity			Roundness		
		Plane 1	Plane 2	Plane 3	Plane 1	Plane 2	Plane 3
Natural Sand, 1.0	–	0.72	0.64	0.48	0.31	0.31	0.39
3D printed, 0.6	DLP	0.71	0.65	0.51	0.48	0.35	0.34
3D printed, 1.98	SLA	0.74	0.69	0.46	0.2	0.23	0.36
3D printed, 4.0	DLP	0.72	0.65	0.47	0.29	0.33	0.36
3D printed, 4.0	SLA	0.70	0.64	0.47	0.32	0.32	0.38

example, for studies that simulate porosity, tortuosity, and pore-fabric of the granular material without gravitational considerations, SLA printing can be adopted. For all other cases, DLP printing provides better representation of the particle morphology, even at smaller scales.

Conclusions

In this paper, mechanical response of 3D-printed planar sheets and geogrids was investigated. The efficacy of different printing methods in reproducing the morphology of sand was also demonstrated using image-based analysis. Following important conclusions drawn based on this study.

- 3D printing provides freedom to customize the geometric, physical, and mechanical characteristics of the materials.
- Geosynthetic sheets of different textures can be printed by changing the direction of printing.
- Among the planar sheets printed in different orientations, diagonally printed sheets showed maximum tensile strength because the two layers comprising the thickness of the sheet were not overlapping, thus eliminating the weaker zones.
- Horizontally printed sheets showed least interfacial shear strengths because of easy sliding of the particles on the fused layers aligned in the direction of shear. Vertically printed and diagonally printed sheets allowed particle interlocking and hence showed higher interface shear strength.
- Geogrids of different aperture shapes can be printed, keeping the same opening area, and changing the design of printing.
- Geogrids with triangular apertures were found to exhibit highest tensile strength due to isotropic resistance offered by them and highest interface shear strength due to interference of ribs and maximum particle interlocking.
- To replicate the exact shape features of sand grains, printing must be done at a scale of 4 or above. DLP is a better technique to print particles compared to SLA.

Funding Funding for this study was provided through SERB Core research grant (CRG/2021/001774) of the Department of Science and Technology, India, and Dam Rehabilitation and Improvement Project (DRIP) of the Ministry of Water Resources (MoWR), Government of India.

Declarations

Conflict of interest The authors do not have any conflict of interest to declare.

References

1. Hull C (1986) Apparatus for production of three-dimensional object by stereolithography. US Patent 4,575,330
2. Thompson MK, Moroni G, Vaneker T, Fadel G, Campbell RI, Gibson I, Bernard A, Schulz J, Graf P, Ahuja B, Martina F (2016) Design for additive manufacturing: trends, opportunities, considerations, and constraints. CIRP Ann 65(2):737–760
3. Hanaor DAH, Gan Y, Revay M, Airey DW, Einav I (2016) 3D printable geomaterials. Géotechnique 66(4):323–332
4. Miskin MZ, Jaeger HM (2013) Adapting granular materials through artificial evolution. Nat Mater 12(4):326–331
5. Ahmed SS, Martinez A (2021) Triaxial compression behavior of 3D printed and natural sands. Granul Matter 23(4):1–21
6. Adamidis O, Alber S, Anastasopoulos I (2019) Assessment of three-dimensional printing of granular media for geotechnical applications. Geotech Test J 43(3):641–659
7. Stathas D, Wang JP, Ling HI (2017) Model geogrids and 3D printing. Geotext Geomembr 45(6):688–696
8. Arab MG, Omar M, Alotaibi E, Mostafa O, Naeem M, Badr O (2020). Bio-inspired 3D-printed honeycomb for soil reinforcement. In: Proceedings of the Geo-Congress 2020: biogeotechnics, Minneapolis, MN, USA, 25–28 February 2020. American Society of Civil Engineers: Reston, VA, USA, pp 262–271
9. Chalmovsky J, Koudela P, Mica L (2020) Reinforcing of sand with 3D printed fibres–review of properties, fabrication of fibres and initial testing programme. In: IOP conference series: materials science and engineering, vol 960, no 3, p 032027
10. ASTM D-882 (2002) Tensile properties of thin plastic sheeting. ASTM International, West Conshohocken
11. ASTM D-6637 (2016) Tensile properties of geogrids by the single or multi-rib tensile method. ASTM International, West Conshohocken
12. Al-Omari RR, Fekheraldin MK (2012) Measurement of tensile properties of geogrids. In: Proceedings of the 2nd international conference on geotechnique: construction materials and environment, 14–16 November 2012, Kuala Lumpur, Malaysia, pp 14–16
13. Guo X, Chen J, Xue J, Zhang Z (2023) Centrifuge model and numerical studies of strip footing on reinforced transparent soils. Geosynth Int. https://doi.org/10.1680/jgein.21.00120

14. Phanikumar BR (2016) Influence of geogrid reinforcement on pullout response of granular pile-anchors (GPAs) in expansive soils. Indian Geotech J 46:437–444
15. Latha GM, Rajagopal K, Krishnaswamy NR (2006) Experimental and theoretical investigations on geocell-supported embankments. Int J Geomech ASCE 6(1):30–35
16. Manohar DR, Anbazhagan P (2021) Shear strength characteristics of geosynthetic reinforced rubber-sand mixtures. Geotext Geomembr 49:910–920
17. Naeini SA, Khalaj M, Izadi E (2013) Interfacial shear strength of silty sand–geogrid composite. Proc Inst Civ Eng Geotech Eng 166(1):67–75
18. Maghool F, Arulrajah A, Mirzababaei M, Suksiripattanapong C, Horpibulsuk S (2020) Interface shear strength properties of geogrid-reinforced steel slags using a large-scale direct shear testing apparatus. Geotext Geomembr 48:625–633
19. Vangla P, Roy N, Gali ML (2018) Image based shape characterization of granular materials and its effect on kinematics of particle motion. Granul Matter 20(1):1–19